Communications Research Centre

STUDY OF THE BEHAVIOR AND STABILITY OF PHASE FRONTS ON SHORT TIME SCALES

by

B.J. Rook

DEPARTMENT OF COMMUNICATIONS
MINISTÈRE DES COMMUNICATIONS

CRC REPORT NO. 1312

This work was sponsored by the Department of National Defence, Research and Development Branch under Project No. 3633G.

OTTAWA, FEBRUARY 1978

COMMUNICATIONS RESEARCH CENTRE

DEPARTMENT OF COMMUNICATIONS
CANADA

STUDY OF THE BEHAVIOR AND STABILITY OF PHASE FRONTS ON SHORT TIME SCALES

by

B.J. Rook

(Radio and Radar Branch)

CRC REPORT NO. 1312

February 1978

OTTAWA

This work was sponsored by the Department of National Defence, Research and Development Branch under Project No. 3633G

TABLE OF CONTENTS

STUDY OF THE BEHAVIOR AND STABILITY OF PHASE FRONTS ON SHORT TIME SCALES

by

B.J. Rook

ABSTRACT

Measurements have been made over an 1181-metre antenna-aperture of the phase of radio waves received after propagation via the ionosphere. Data were obtained for two paths: the first a 453 km, mid-latitude link, the second a 1950 km, sub-auroral link. In both cases, the signals from the individual elements in the array were sampled at intervals of about 20 milliseconds. The decorrelation of phase-front shape with increasing time displacement was then calculated. For the mid-latitude path data, it was found that the mean time for the wave front to decorrelate to 0.7 was about 5 seconds, while for the longer, higher-latitude path, the corresponding time was approximately 1.1 seconds.

1. INTRODUCTION

Long range transmissions at HF are possible because of the existence of the ionospheric medium. However, since this medium is stratified, multipath propagation occurs which results in an interference pattern that varies in space and time over the antenna aperture at the receiving site. For direction-finding, the existence of more than one ray results in non-planar phase fronts and hence the observed bearing deviates from the great-circle direction, resulting in inaccuracies in the position fixing of the source of the transmissions.

Hayden[1] has shown that if there are two rays present, the otherwise plane equiphase surface of the ray with the greater amplitude becomes corrugated, the magnitude of the corrugations depending upon the ratio of the

amplitudes of the two rays. Furthermore, the spacing of these corrugations as measured along the equiphase surface is a function of the angle between the two rays. In the following section, after a brief description of the experimental arrangements, these concepts are examined along with the effects of Doppler shift and angle-change in preparation for the examination of the data. Following this, a correlation technique is used in determining, statistically, the stability of wavefronts with time.

2. EXPERIMENTAL ARRANGEMENTS

The Communications Research Centre's (CRC) high frequency direction finding (HFDF) facility[2,3] is a highly sophisticated research tool designed for the accurate measurement of direction of arrival and of time delay of HF signals. It was developed for the purpose of gaining further insight into the propagation mechanisms which give rise to bearing inaccuracies. The results presented here were obtained using 42 elements non-uniformally distributed over a total aperture of 1181 metres, the principal spacings being 15.24 and 38.10 metres.

Each element of the antenna array is connected to a separate phase-matched receiver, with quadrature product detector outputs. The receiver outputs were digitized and scanned sequentially at a rate of the order of 50 scans/sec. These digitized outputs, which may be regarded as replicas of the real and imaginary parts of the wavefield as sampled at the element positions, were then recorded on magnetic tape for subsequent processing by computer. The complete system is under the control of an on-line mini-computer.

Interference patterns were observed on two links: one from Boston, Massachusetts, to Ottawa, a mid-latitude link, with a great-circle path length of 453 km; and the other from Churchill, Manitoba, to Ottawa, a sub-auroral link, with a great-circle path length of 1950 km. The sub-auroral zone link has been defined as such since Churchill is near the maximum of the auroral zone, but the ionospheric-controlling point lies south of the auroral-zone. The measuring array was aligned 9.98° and 7.76° off-path to the mid-latitude and sub-auroral-zone links respectively. Thus, the interference patterns in both cases were observed approximately on the plane of the great-circle path from the transmitter to the receiver.

3. CHARACTERISTICS OF WAVE-INTERFERENCE PATTERNS

3.1 PERIODICITY

The behavior of interference patterns is most simply illustrated if the observing antenna array is aligned along the equiphase surface of the stronger ray. (For completeness, Appendix 1 gives the general solution for rays (wave vectors) at arbitrary angles with respect to the antenna array). If a second ray, which will be called the interfering ray, is present, its equiphase plane surface is positioned at an angle $\psi_2 - \pi/2$ to the axis of the antenna array,

where ψ_2 is defined in Figure 1. The combination of these two rays will produce an interference (fading) pattern along the length of the array. The origin in Figure 1 is considered to be the point at which both rays are in phase.

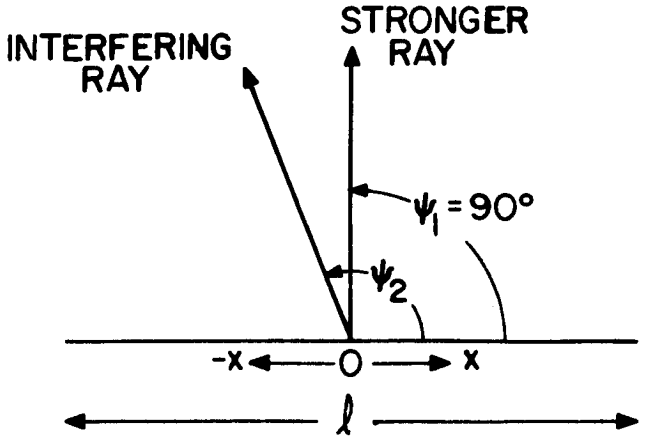

Figure 1. Illustration of the Antenna Array of Length ℓ Aligned along the Equiphase Plane Surface of the Stronger Ray.

This interference pattern may be deduced from the phasor diagram which is shown in Figure 2. The phasor, corresponding to the stronger ray, is represented by the horizontal line labelled 'A' with a magnitude of unity. This phasor is independent of the distance along the array because the equi-phase surface of the stronger ray is parallel to the antenna array. However, the phasor labelled 'B' corresponding to the interfering ray of magnitude r ($r < 1$) does rotate with distance. Thus, the resultant phase angle β is the phase that would be measured as a function of distance along the array. One can see from Figure 2 that when the two rays are in phase, their amplitudes will add and conversely when the two rays are in anti-phase, their amplitudes will subtract.

The phase angle $\phi(x)$ of the interfering ray is given by

$$\phi(x) = \frac{2\pi}{\lambda} x \cos \psi_2 \qquad (1)$$

therefore, the period x_p measured along the array in which $\phi(x)$ completes one revolution and hence in which the interference pattern will repeat, is given by

$$x_p = \frac{\lambda}{\cos \psi_2} . \qquad (2)$$

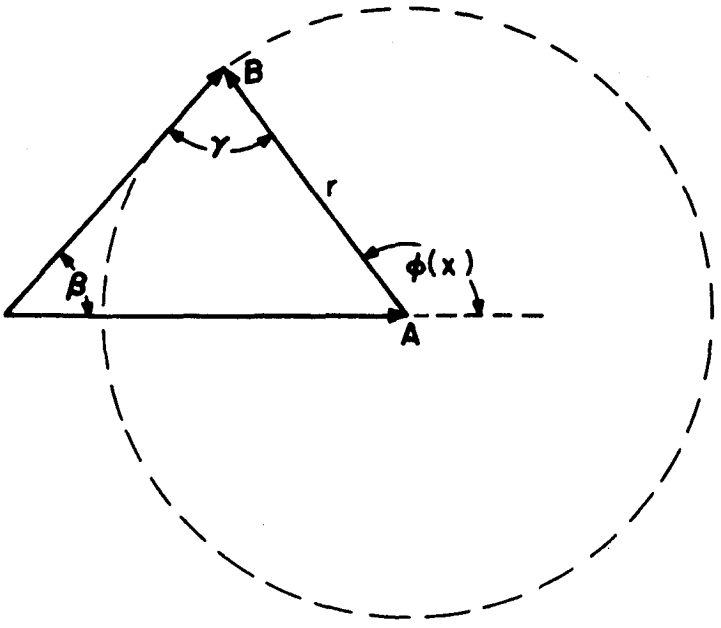

Figure 2. Phasor Diagram Representation of the Interference Pattern along the Antenna Array.

3.2 PHASE DEVIATION

From Figure 2, the maximum phase deviation of the resultant phasor occurs when γ is 90° or 270° (see Appendix 1). Thus, the maximum phase deviation occurs when

$$\cos \phi = -r \tag{3}$$

and will have the values

$$\beta_{max} = \pm \sin^{-1} r. \tag{4}$$

Theoretical plots of interference patterns, that is plots of the phase angle β as a function of distance, are shown in Figure 3. These results were obtained using the general solution (see Appendix 1, eqn. 1-II) with t = 0, from which β is given by

$$\beta = \phi - kx \cos\psi_1 = \tan^{-1}\left[\frac{r \sin (kx[\cos\psi_2 - \cos\psi_1])}{1 + r \cos(kx[\cos\psi_2 - \cos\psi_1])}\right] \tag{5}$$

The parameters used to obtain these results were r = 0.9, λ = 50.0 metres and $\psi_2 - \psi_1 = 20.0°$. In these results, the magnitude of the peak-to-peak phase deviation $2\beta_{max}$ is 128.3° and the minimum period x_p is 146.2 metres. Since the properties of the waves are the same for all the plots, these particular examples show the effect of varying the receiving array angle. Note that as ψ_1 decreases from 90.0° the period of the interference pattern increases.

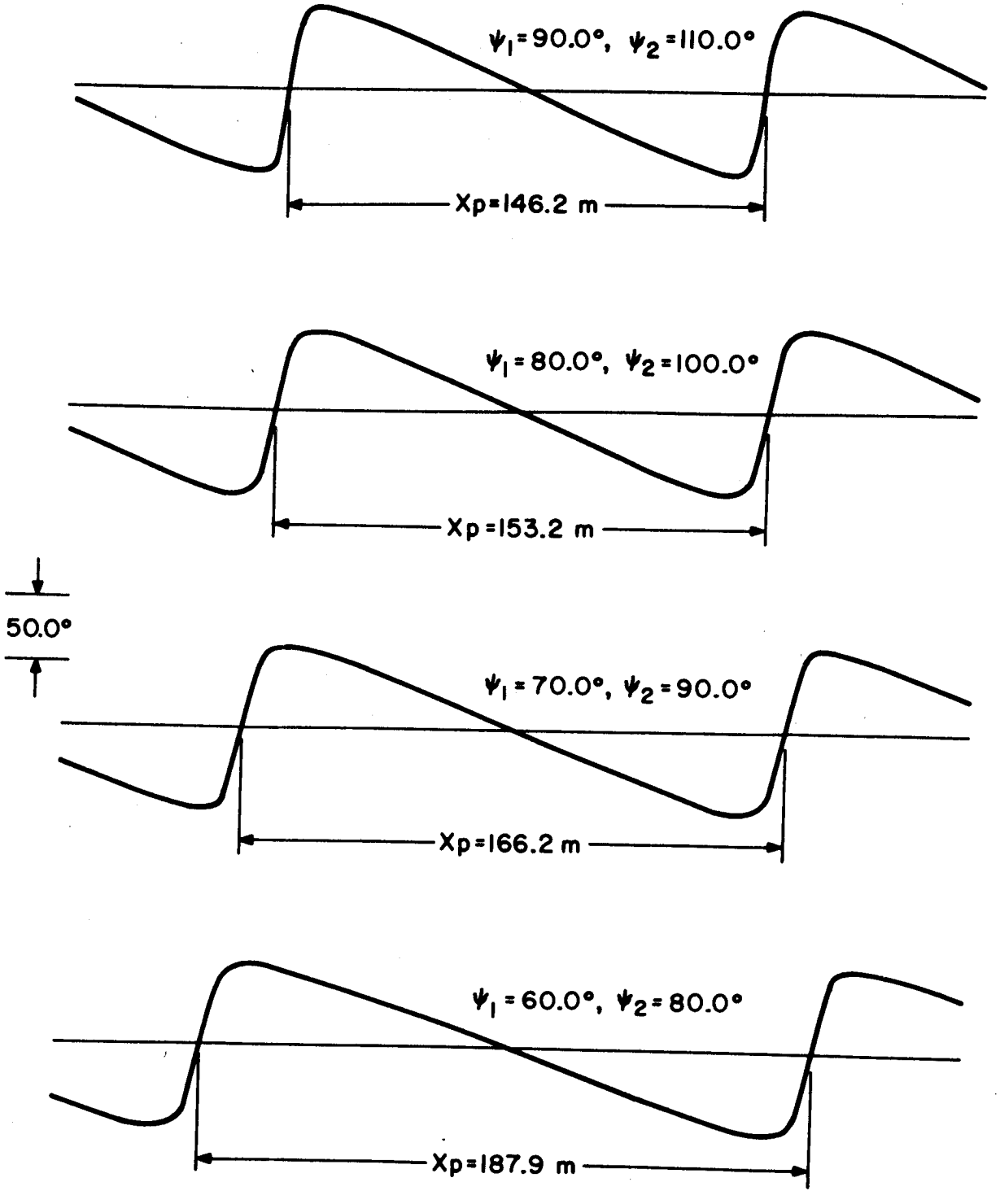

Figure 3. Theoretical Plots of Interference Patterns.

Although only two rays have been considered in deriving the resultant interference pattern in Figure 3, one cannot exclude the possibility of multi-ray paths. The interference pattern which results when three or more rays are present is very complex and the period usually large. Examples of phase-front measurements when three or more rays are present are illustrated and discussed later in the text. However, for the remainder of the theoretical discussion, only two rays are considered where the stronger ray is perpendicular to the antenna array.

3.3 PHASE-PATH LENGTH CHANGE WITH TIME

If the phase-path length of one ray (say the interfering ray) is increasing or decreasing with time, relative to the other, that is if there exists a Doppler shift, the phasor rotates with time and the expression for phase becomes

$$\phi = \frac{2\pi}{\lambda} x \cos \psi_2 - \phi_o(t) \tag{6}$$

where ϕ_o is the phase at the origin. The points of constant phase and hence the interference pattern, then moves along the array with a velocity

$$\frac{dx}{dt} = \frac{\lambda}{2\pi \cos\psi_2} \frac{d\phi_o}{dt} = \frac{\lambda \Delta f}{\cos \psi_2} , \tag{7}$$

where Δf is the Doppler frequency shift.

3.4 CHANGE IN THE ANGLE ψ_2 WITH TIME

If the phase path remains constant at the origin but the angle ψ_2 is changing with time, then the velocity of a constant phase point is obtained from the time derivative of eqn. (6):

$$\frac{dx}{dt} = x \tan \psi_2 \frac{d\psi_2}{dt} \tag{8}$$

The results of Section 3 can now be summarized as follows: The spacing of the irregularities as measured orthogonal to the stronger ray depends only on the angle between the two rays; the maximum phase deviation depends only on the relative amplitudes of the two rays; a Doppler shift on one of the rays relative to the other produces a drifting motion of the interference pattern along the phase front; and a change in the angle between the rays produces an expansion or a contraction in the period of the interference pattern. The data will now be examined for these and other effects.

4. FEATURES OF THE OBSERVATIONS

4.1 GENERAL DESCRIPTION

In the results which follow, time sequences of the phase variation along the array are plotted (e.g., Figure 4). The array was scanned at intervals of 19.42 milliseconds (hereafter approximated as 20 milliseconds) and all phase plots in the figures are separated by some multiple of this basic period. Each array scan required 1.9 milliseconds to complete. The relatively minor effects of this finite array scan time were compensated for in the later computer processing of the data.

In each case, the mean slope as determined by the least-squares fit of a straight line to the data has been subtracted leaving only the deviations about the straight line. The time sequence of the phase plots runs from top to bottom in the figures. Thus in Figure 4, the top line represents the deviation in phase as a function of distance along the array and the second line represents the phase deviation 20 ms later, etc.. Several hundred phase fronts were examined and samples where chosen in order to demonstrate particular features in the data.

4.2 IONOSPHERIC MODE DESIGNATIONS

Before proceeding to discuss the results, a list of symbols used in labelling the various modes of propagation on the ionograms are given below:

E_s	sporadic E
EL	low-angle E-layer
EH	high-angle E-layer
F1(o)L	low-angle F_1-layer o-mode
F1(o)H	high-angle F_1-layer o-mode
F1(x)L	low-angle F_1-layer x-mode
F1(x)H	high-angle F_1-layer x-mode
F2(o)L	low-angle F_2-layer o-mode
F2(o)H	high-angle F_2-layer o-mode
F2(x)L	low-angle F_2-layer x-mode
F2(x)H	high-angle F_2-layer x-mode

where the o and x modes are unresolved, the letters o and x have been omitted from the symbols. Also, measurements of the angle between the incoming ray and the axis of the antenna array, called the cone angle in this report, were determined from time-delay-resolved measurements which ran concurrently with this experiment. The use of the term cone angle is appropriate here since the incoming ray can be anywhere on the surface of a cone symmetric about the array axis.

4.3 DISCUSSION OF RESULTS FROM THE MID-LATITUDE LINK

Figure 4 shows the relative phase variation along the array measured every 20 milliseconds over the Boston-Ottawa link. The results show clearly the phase deviation which results when two propagation paths are present. An

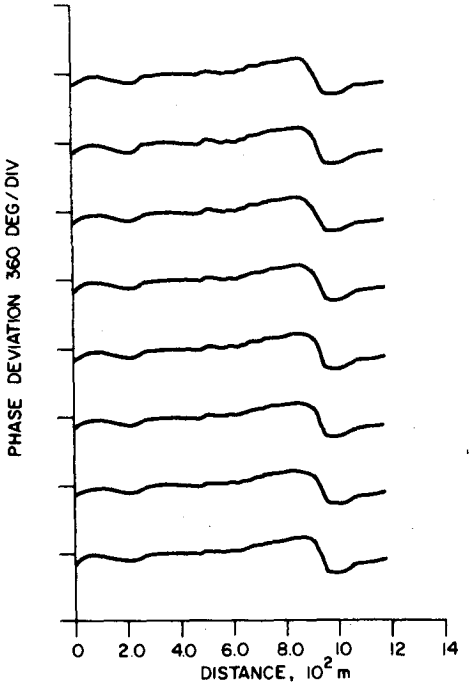

Figure 4. Plots of phase fronts taken every 20 milliseconds over the Boston-Ottawa link on February 16, 1975 at 15:32:15 EST. Frequency of operation is 5.85 MHz.

examination of an ionogram for this time (see Figure 5) indicates that for the frequency of operation (5.85 MHz), only two modes of propagation were significant, namely, low-angle F_2-layer o and x-modes (F2(o)L, F2(x)L) with cone angles measured to be 46.8° and 42.3° respectively. The period of the interference pattern is not visible over the length of the antenna array consistent with the angle between the two rays being small (<5.0°). Another point to note is that there is no discernible drifting motion of the interference pattern with time over the complete time block of 140 milliseconds. This multipath propagation of the F-region, although interesting, is not typical of what has been observed on this link.

A more typical result is shown in Figure 6. This result shows samples of the instantaneous phase fronts every 120 milliseconds for a total time block of 0.84 seconds. This example shows clearly the resultant interference pattern when at least five modes of propagation are present. An ionogram for this time period is shown in Figure 7. The dominant modes of propagation at the frequency of interest (5.25 MHz) are sporadic E(E_s), low-angle E-layer (EL), high-angle E-layer (EH), low-angle F_1-layer o-mode (F1(o)L), and low-angle F_1-layer x-mode (F1(x)L) with cone angles measured to be 22.1°, 26.9°, 29.6°, 45.3° and 46.8° respectively. The darkness of the trace in this ionogram indicates that there were several modes of propagation with similar intensities and this accounts for the rather large phase deviation about the mean slope. One can see from these measurements that the phase fronts are complex in form with a resulting period which extends well beyond the length of the aperture. It will also be noted that there is no discernible drift of the interference pattern with time over the complete time block of 0.84 seconds. However, the form of the phase front is slowly changing indicating that the relative amplitudes of the rays are slowly changing with time. Examination of many

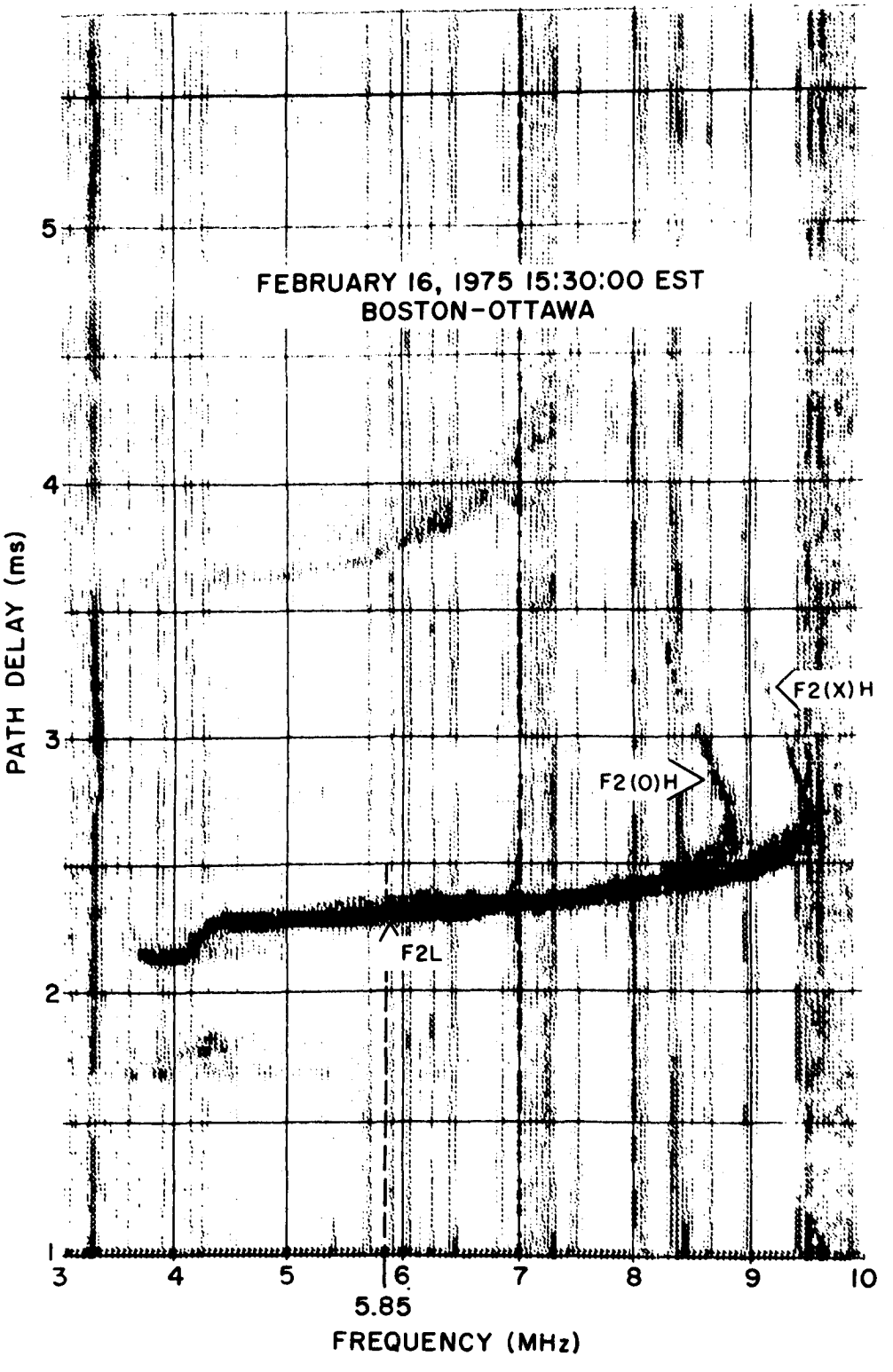

Figure 5. Ionogram Measured over the Boston-Ottawa Link on February 16, 1975 at 15:30:00 EST.

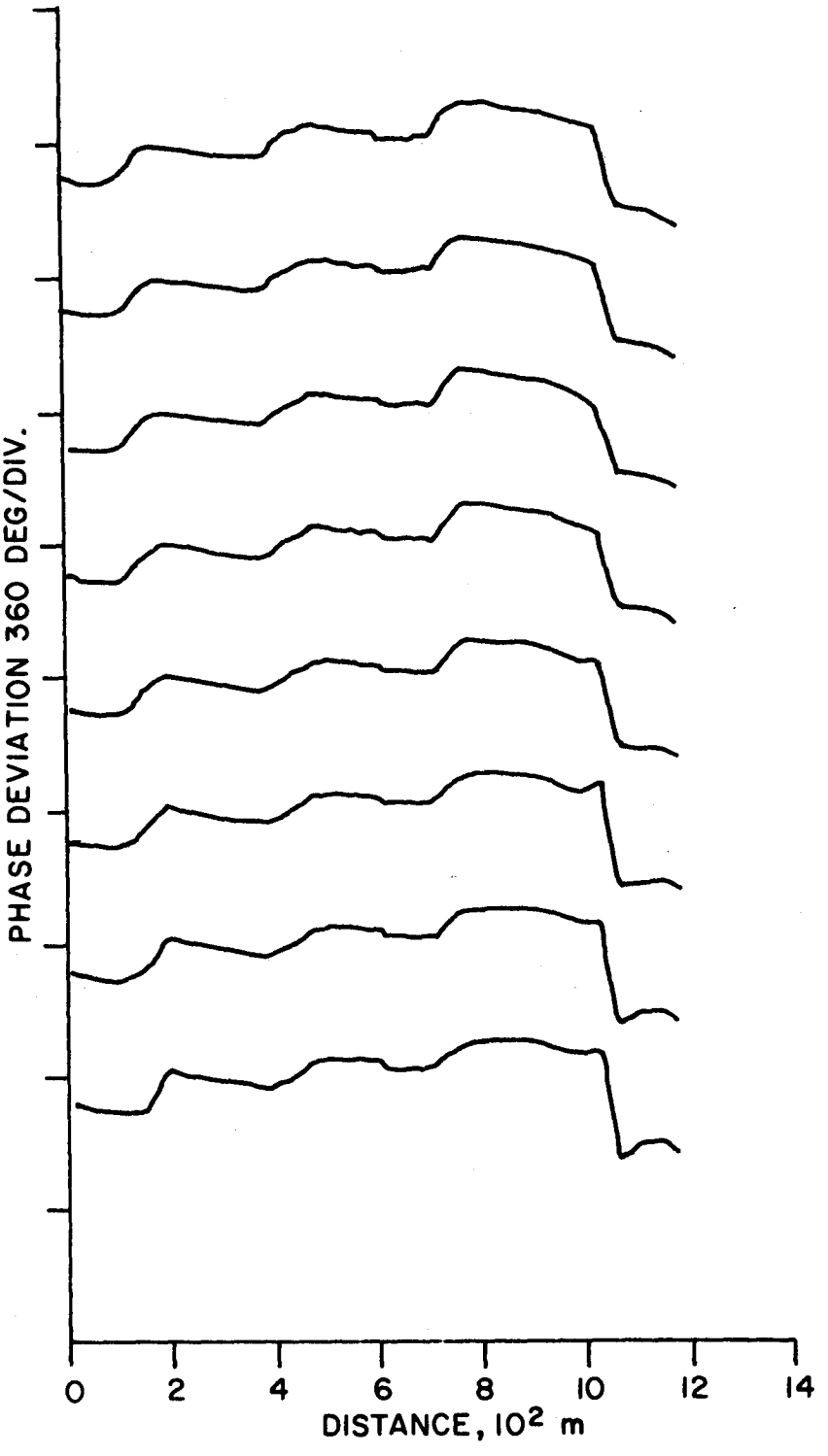

Figure 6. Plots of phase fronts taken every 120 milliseconds over the Boston-Ottawa link on February 18, 1975 at 11:29:15 EST. Frequency of operation is 5.25 MHz.

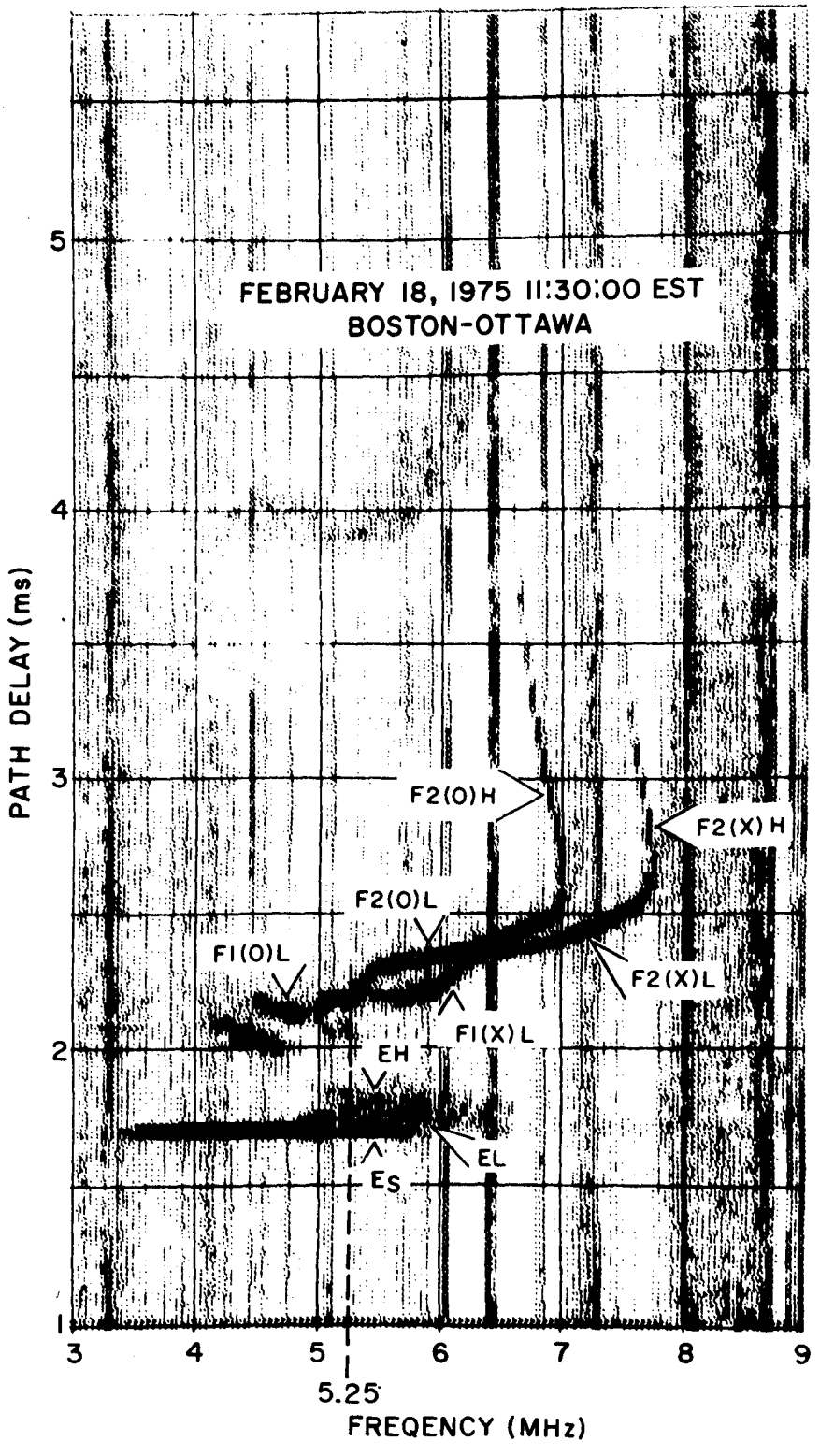

Figure 7. Ionogram Measured over the Boston-Ottawa Link on February 18, 1975 at 11:30:00 EST.

phase fonts indicates that this change in relative magnitude is the most common cause of change in the interference pattern on this mid-latitude link.

In Figure 8, a similar result is shown except that the time interval between successive scans of the instantaneous phase fronts is 380 milliseconds for a total time block of 3.04 seconds. An ionogram for this time period is shown in Figure 9. The dominant modes of propagation at the frequency of interest (6.04 MHz) are sporadic E(E_s), low-angle E-layer (EL), low-angle F_2-layer o-mode (F2(O)L) and low-angle F_2-layer x-mode (F2(x)L) with cone angle measurements of 22.8°, 27.2°, 45.1° and 48.1° respectively.

It will be noted that the magnitude of the phase deviations remains fairly constant but the interference pattern is drifting slowly along the array indicating the presence of a Doppler-shift on at least one mode. This drifting motion is illustrated in Figure 8 by noting a fixed point in space (dashed line A-B) and observing the drift. The slowness of this drifting motion is typical of what has been observed over the Boston-Ottawa link.

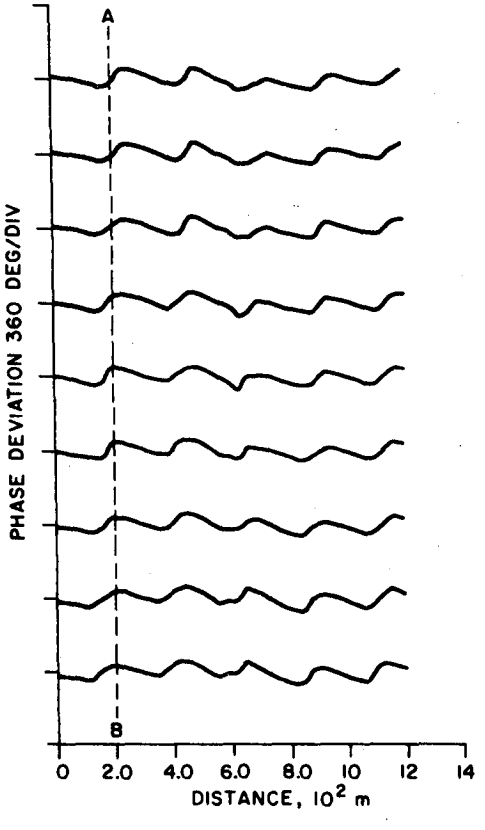

Figure 8. Plots of phase fronts taken every 380 milliseconds over the Boston-Ottawa link on February 18, 1975 at 12:44:15 EST. Frequency of operation is 6.04 MHz.

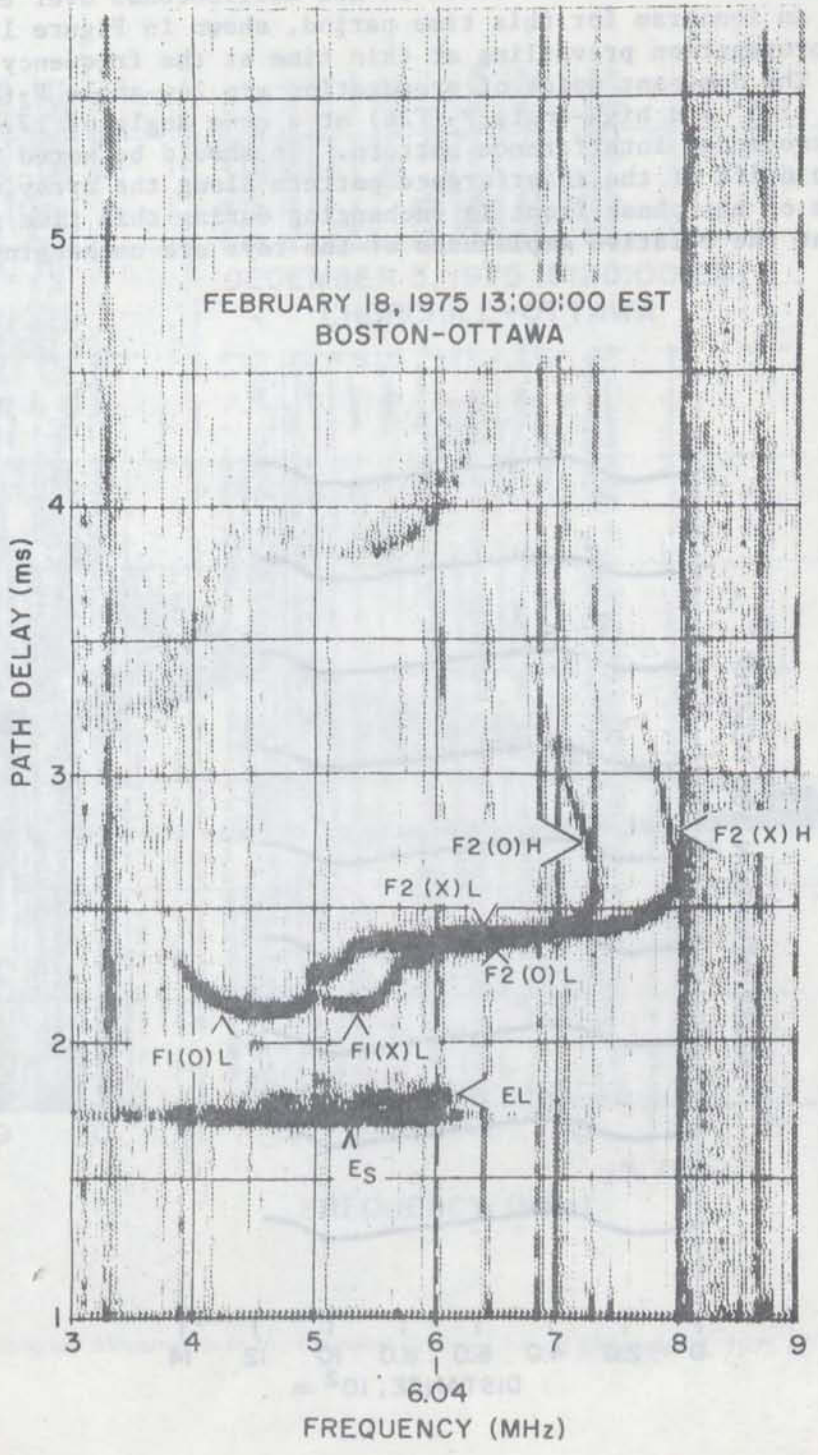

Figure 9. Ionogram Measured over the Boston-Ottawa Link on February 18, 1975 at 13:00:00 EST.

4.4 DISCUSSION OF RESULTS FROM THE SUB-AURORAL-ZONE LINK

Figure 10 shows plots of the instantaneous phase fronts taken every 20 milliseconds for a total time block of 160 milliseconds over the Churchill-Ottawa link. An ionogram for this time period, shown in Figure 11, illustrates the modes of propagation prevailing at this time at the frequency of interest (15.75 MHz). The dominant modes of propagation are low-angle F_2(F2L) at a cone angle of 11.5° and high-angle F_2(F2H) at a cone angle of 17.2° resulting in a typical two-moded interference pattern. It should be noted that there is no discernable drift of the interference pattern along the array with time. Also, the form of the phase front is unchanging during this time period, indicating that the relative amplitudes of the rays are unchanging.

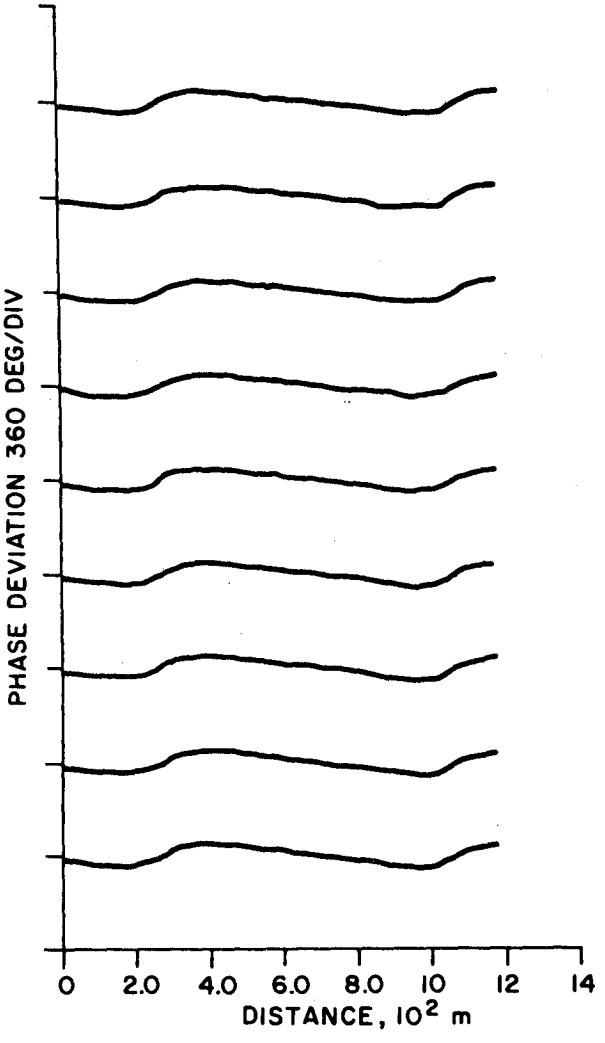

Figure 10. Plots of phase fronts taken every 20 milliseconds over the Churchill-Ottawa link on December 3, 1975 at 15:32:20 EST. Frequency of operation is 15.75 MHz.

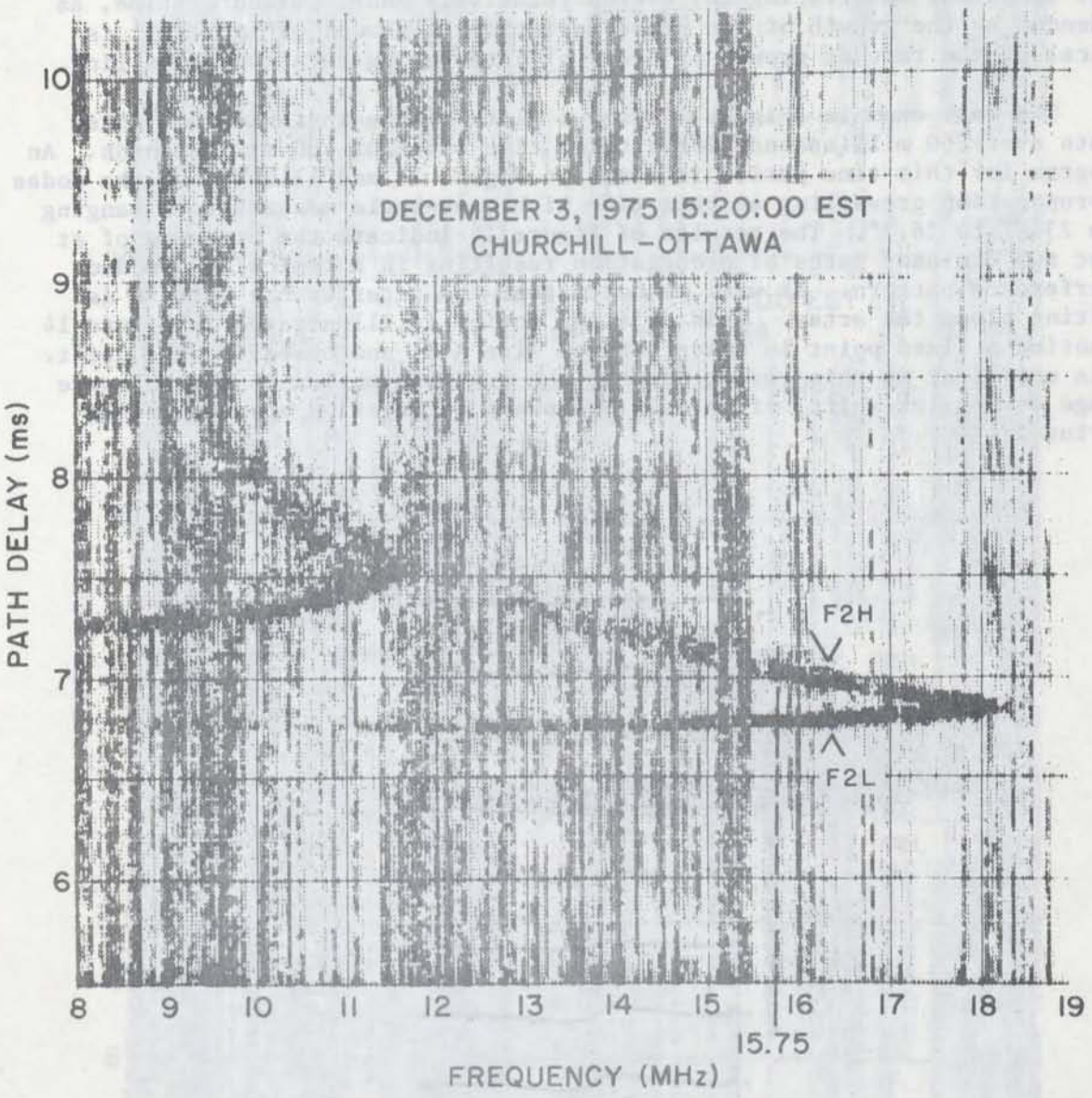

Figure 11. Ionogram Measured over the Churchill-Ottawa Link on December 3, 1975 at 15:20:00 EST.

Figure 12 shows another set of plots of the instantaneous phase fronts taken every 20 milliseconds over the same link as above. An ionogram for this time period is shown in Figure 13 and illustrates the ionospheric conditions prevailing at this time (i.e., Spread F conditions) with cone angles ranging from 18.1° to 23.4°. The resultant phase plots in Figure 12 show the growth of at least one interfering ray over a relatively short period of time, as evidenced by the growth of the phase deviation as shown. This result is typical of the rate of growth or decay of interfering rays over this link.

The last example (Figure 14) shows plots of the instantaneous phase fronts every 60 milliseconds for a total time block of 480 milliseconds. An ionogram for this time period is shown in Figure 15 and illustrates the modes of propagation prevailing at this time with cone-angle measurements ranging from 23.9° to 26.7°. The results of Figure 14 indicate the presence of at least two dominant paths of propagation resulting in a typical two-moded interference pattern. It will be noted that the interference pattern is drifting along the array. This drifting motion is illustrated in Figure 14 by noting a fixed point in space (dashed line A-B) and observing the drift. It is not clear in this result whether the drifting motion is due to angle change or Doppler-shift, since only one phase corrugation appears in the aperture.

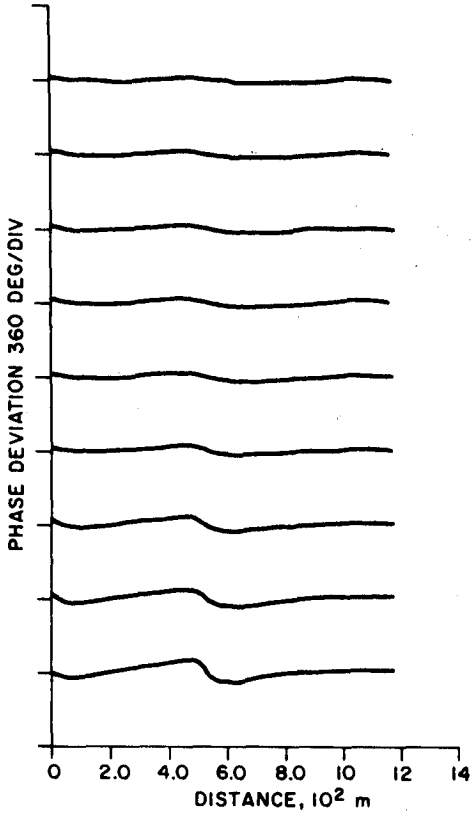

Figure 12. Plots of phase fronts taken every 20 milliseconds over the Churchill-Ottawa link on November 29, 1975 at 14:25:20 EST. Frequency of operation is 13.7 MHz.

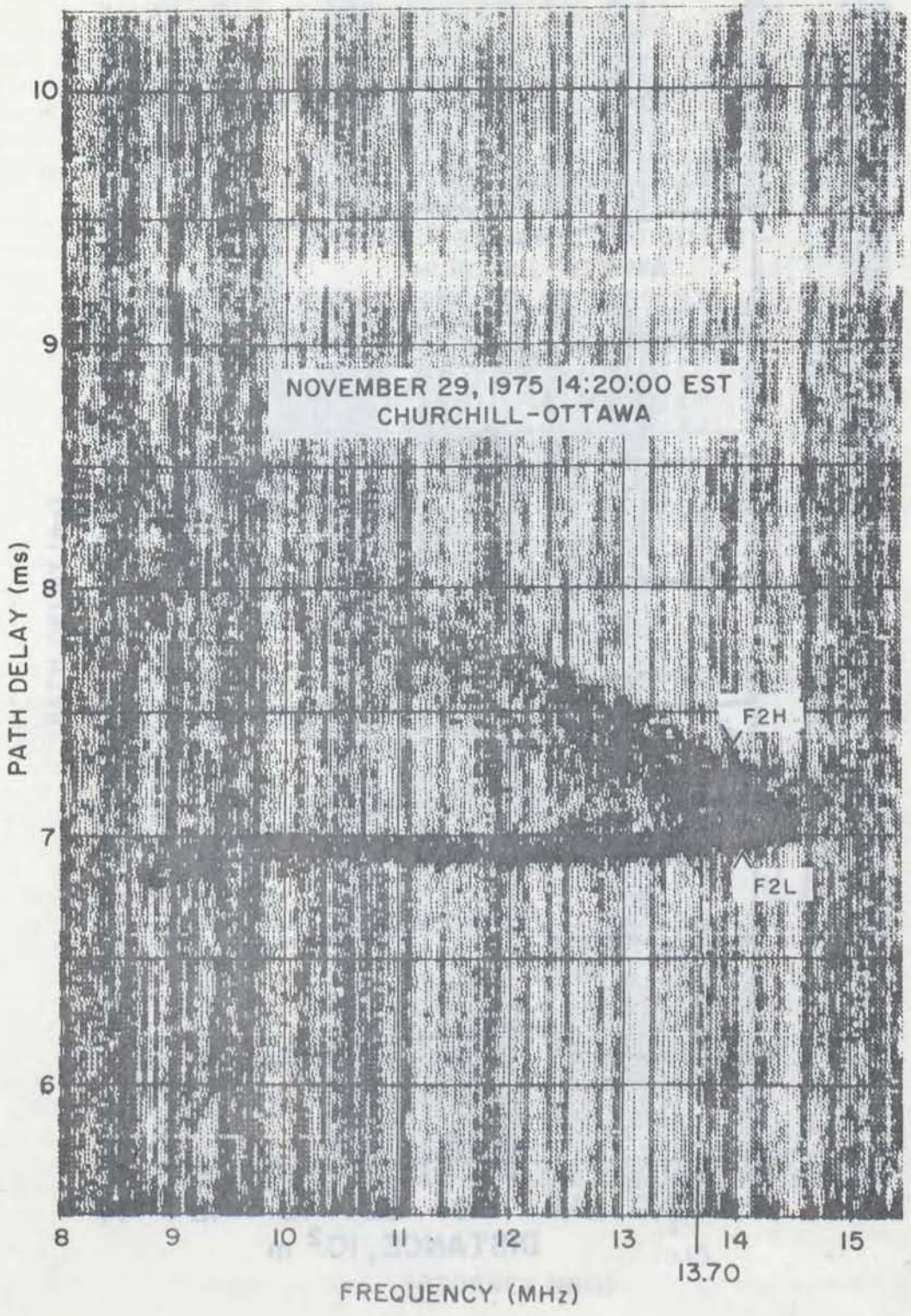

Figure 13. Ionogram Measured over the Churchill-Ottawa Link on November 29, 1975 at 14:20:00 EST.

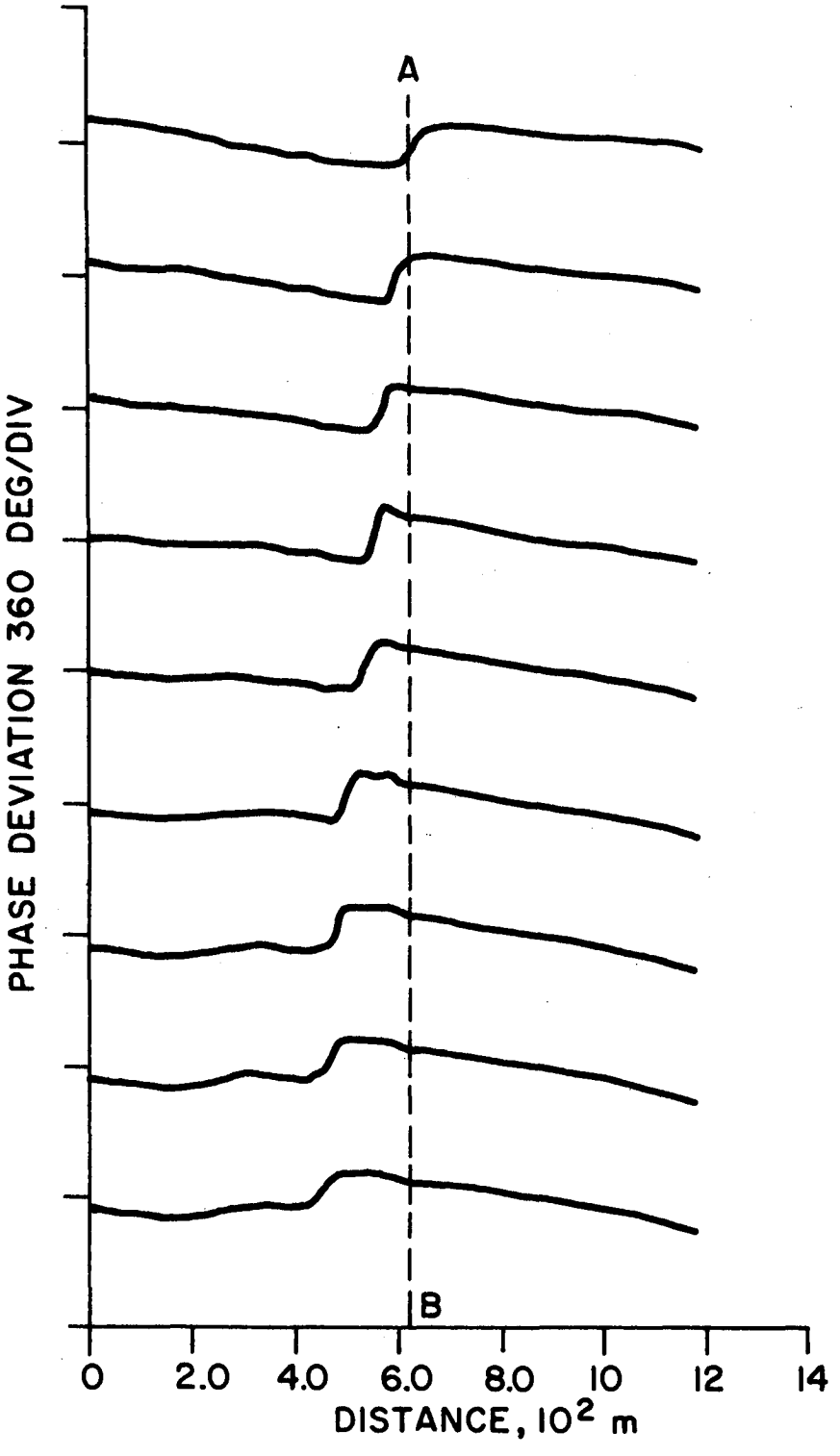

Figure 14. Plots of phase fronts taken every 60 milliseconds over the Churchill-Ottawa link on November 29, 1975 at 12:08:20 EST. Frequency of operation is 10.15 MHz.

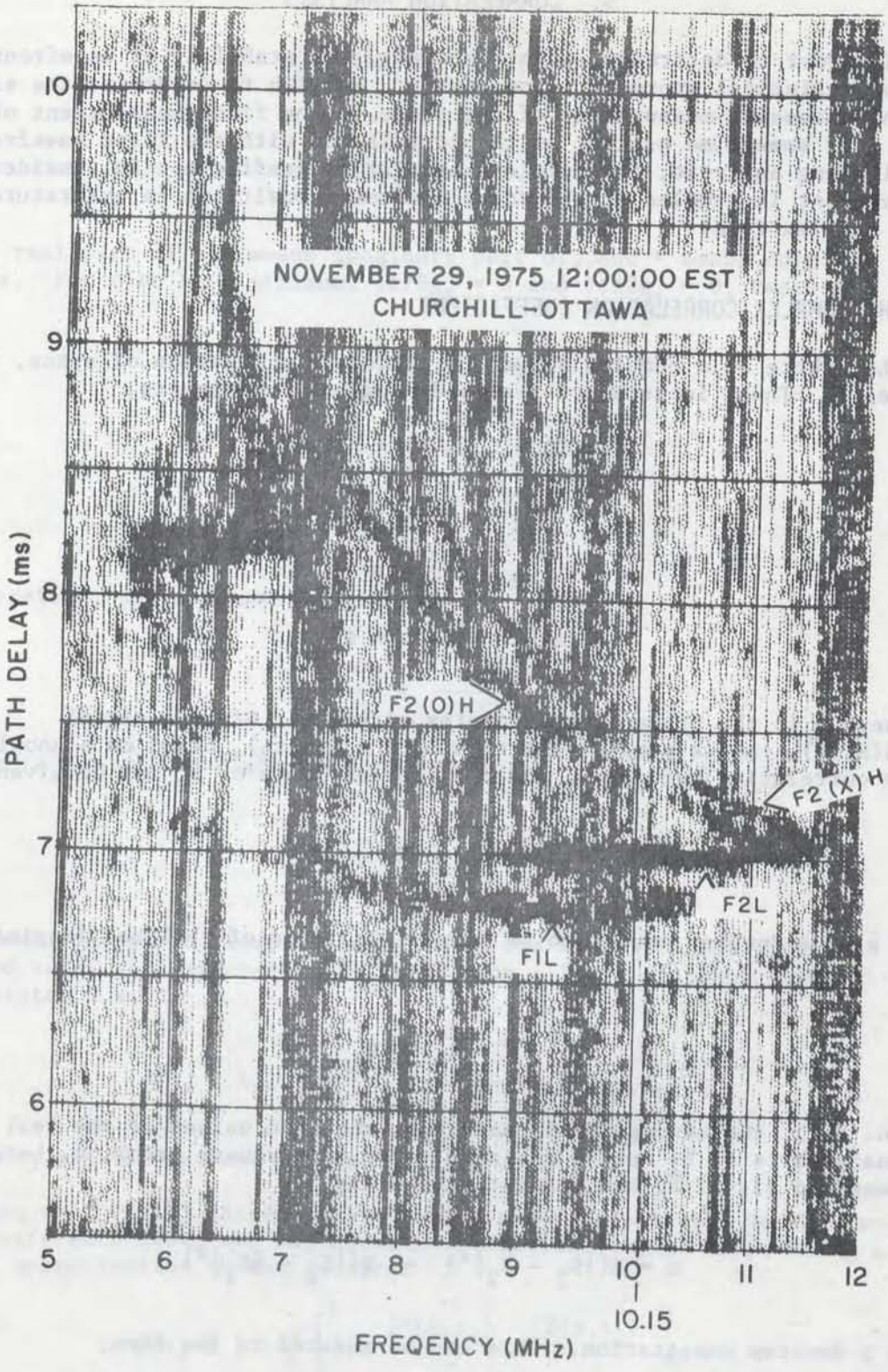

Figure 15. Ionogram Measured over the Churchill-Ottawa Link on November 29, 1975 at 12:00:00 EST.

5. CORRELATION ANALYSIS

In order to determine, quantitatively, the stability of wavefronts with time, a statistical approach is necessary. We wish to determine the similarity of each successive measurement of the phase to the first measurement of the phases over some time period, or the correlation with the first wavefront. In the following analysis, the complex correlation coefficient is considered since the wavefront is sampled at the antenna element positions in quadrature form (i.e., complex form).

5.1 THE COMPLEX CORRELATION COEFFICIENT

Let there be a complex signal, S, which is a function of space, x, and of time, t. Then, in terms of real and imaginary components,

$$S(x,t) = S_R(x,t) + jS_1(x,t) \tag{9}$$

where

$$S_R = |S| \cos \phi \tag{10}$$

$$S_I = |S| \sin \phi \tag{11}$$

and where ϕ is the phase of the complex signal S. Given a signal $S_1 = S(x,t_1)$, can we predict the signal $S_2 = S(x,t_2)$, based on a knowledge of the correlation between S_1 and S_2? The estimate of S_2 may be given by

$$\hat{S}_2 = \tilde{g}S_1 \tag{12}$$

where $\tilde{g}$ is a complex number to be found. In terms of real and imaginary parts,

$$\tilde{g} = g_R + jg_1 \tag{13}$$

In eqn. (12), the assumption is made that the mean values of the real and imaginary parts of S_1 and S_2 are zero. The mean square error, ε, between the measured signal S_2 and its estimate $\hat{S}_2$ is

$$\varepsilon = E\{|S_2 - \hat{S}_2|^2\} = E\{|S_2 - \tilde{g}S_1|^2\} \tag{14}$$

where E denotes expectation. This can be reduced to the form,

$$\varepsilon = \sigma_2^2 + (g_R^2 + g_1^2)\,\sigma_1^2 - 2g_R \,\mathrm{Re}\, E\{S_1 S_2^*\} + 2g_1 \,\mathrm{Im}\, E\{S_1 S_2^*\} \tag{15}$$

where

$$\sigma_1^2 = E\{S_1 S_1^*\} = |S_1|^2 \tag{16}$$

and

$$\sigma_2^2 = E\{S_2 S_2^*\} = |S_2|^2 \tag{17}$$

Re means real part of, Im means imaginary part of, and * means complex conjugate. For ε to be a minimum, $\partial\varepsilon/\partial g_R = 0$ and $\partial\varepsilon/\partial g_I = 0$, resulting in

$$g_R = \frac{1}{\sigma_1^2} \text{ Re } E\{S_1 S_2^*\} \tag{18}$$

and

$$g_I = -\frac{1}{\sigma_1^2} \text{ Im } E\{S_1 S_2^*\} \tag{19}$$

Therefore, the estimate $\hat{S}_2$ is given by

$$\hat{S}_2 = \frac{\sigma_2}{\sigma_1} S_1 \frac{E\{S_1^* S_2\}}{\sigma_1 \sigma_2} \tag{20}$$

where the factor on the right-hand side

$$\frac{E\{S_1^* S_2\}}{\sigma_1 \sigma_2} = \frac{\sigma_1}{\sigma_2} \tilde{g} = \tilde{\rho} \tag{21}$$

may be identified as the complex correlation coefficient. For the data considered here, the expectation is taken over all the available spatial sample points, i.e.,

$$\tilde{\rho}(t_2 - t_1) = \frac{1}{\sigma_1 \sigma_2} \sum_{i=1}^{N} S^*(x_i, t_1) S(x_i, t_2) \tag{22}$$

where the x_i are the antenna element positions.

Using eqn. (I-11) (Appendix I) for the phase deviation β in the two-mode intereference case, one may compute theoretical values of $\tilde{\rho}$, using a numerical approximation to the integral

$$\tilde{\rho}(t_2 - t_1) = \frac{1}{L} \int_0^L e^{-j\beta(x,t_1)} e^{j\beta(x,t_2)} \, dx \tag{23}$$

where the interval L is taken as 1 cycle of the interference pattern, i.e., $L = X_p$. In practice the aperture L is fixed and the result for experimental data will differ from the theoretical, particularly if $L < X_p$.

Figure 16 shows the calculated magnitude and phase of $\tilde{\rho}$ as a function of $\omega_d\tau$ for various amplitude ratios r. This corresponds to the case where one of the components is doppler shifted. Figure 17 shows the magnitude of $\tilde{\rho}$ as a function of r, for various initial values of r, denoted r_1. This corresponds to the case where one or both of the amplitudes are varying but there is no doppler shift or angle change. For the special, limiting case of equal mode amplitudes it is shown in Appendix II that the complex correlation coefficient $\tilde{\rho}$ is given by

$$\tilde{\rho}(\tau) = \left(1 - \frac{\omega_d\tau}{\pi}\right) e^{-j\frac{\omega_d\tau}{2}}, \quad 0 \leq \tau \leq \frac{2\pi}{\omega_d} \tag{24}$$

and $\tilde{\rho}(\tau)$ repeats periodically beyond this.
For r = 1, it should be noted in Figure 16 that as $\omega\tau \to \pi$, $|\tilde{\rho}| \to 0$, and the corresponding phase angle $\phi \to \pi/2$ (i.e., half the value of the phase $\omega_d\tau$). Note also that for small amplitude ratios r, $|\tilde{\rho}|$ remains close to its limiting value of 1. In the limit of no wave interference, the wavefronts remain perfectly correlated for all time.

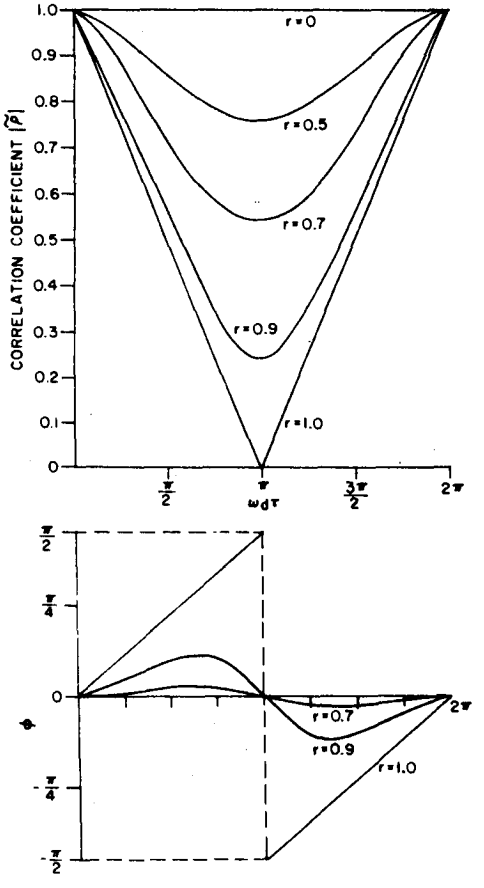

Figure 16. Theoretical Plots of the Magnitude and Phase of the Complex Correlation Coefficient $\tilde{\rho}$ against $\omega_d\tau$ for Various Values of r.

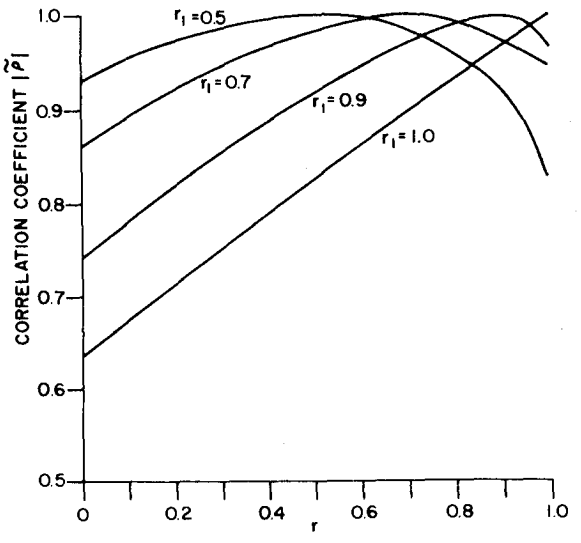

Figure 17. Theoretical Plots of the Magnitude of the Complex Correlation Coefficient $\tilde{\rho}$ against r for Various Initial Values of r, denoted r_1.

6. CORRELATION RESULTS

In the experimental results which follow, the complex correlation coefficient has been computed from measurements of the signal phases only and thus $\sigma_1 = \sigma_2 = 1$. Also, the mean phase slope has been removed from each phase front measurement independently, prior to the computation of the correlation coefficient. The correlation coefficient was then determined (see eqn. (22)) by comparing successive measurements of the phase front to that of the first measured phase front in a contiguous set of phase-front recordings.

Figure 18 and Figure 19 show plots of the correlation coefficient against time determined from phase front measurements over the Boston-Ottawa and Churchill-Ottawa links respectively. A sample of phase fronts which were present at the time are illustrated in Figure 8 and Figure 14. These two examples were chosen because both results contain the combination of a drifting motion and a time variation in the magnitude of the phase deviation. It will be noted that the correlation coefficient decreases much more rapidly over the sub-auroral-zone link than that over the mid-latitude link.

A measure of phase-front stability is the time to decorrelate to a specified value. Figures 20 and 21 show the cumulative probability distributions for the time to decorrelate to 0.9 and 0.7 respectively, for the two links involved. It may be noted from Figures 20 and 21 that there is considerable day-to-day variation in the time to decorrelate to a specified value. However, average values, which may be taken as representative for 50% of the phase fronts to decorrelate to 0.9 and 0.7, are shown for the two links in Table 1. For a correlation coefficient of 0.9, 50% of the occurrences fell within an average time of 0.4 seconds for the Churchill-Ottawa link, whereas, 50% of the occurrences fell within an average time of 2.0 seconds for the Boston-Ottawa link. Also, for a correlation coefficient of 0.7, 50%

fell within an average time of 1.1 seconds for the Churchill-Ottawa link and 5.0 seconds for the Boston-Ottawa link. (It should be noted that the average time of 5.0 seconds quoted for Boston-Ottawa was determined by extrapolating the curves out to the 50% level.) Thus, for a correlation coefficient of 0.9, the average time in which the wavefront may be regarded as stable is 2.0 seconds for the mid-latitude path and 0.4 seconds for the sub-auroral-zone path. Similarly, for a correlation coefficient of 0.7, the stability of the wavefront is 5.0 seconds for the mid-latitude path and 1.1 seconds for the sub-auroral-zone path. Thus the mid-latitude link remains stable approximately five times as long as the sub-auroral-zone link.

TABLE 1

Comparison of the Average Time in which the Wavefront Decorrelated to 0.9 and 0.7 for the Two Links

Correlation Coefficient	Churchill-Ottawa Time of Occurrences Seconds	Boston-Ottawa Time of Occurrences Seconds
0.9	0.4	2.0
0.7	1.1	5.0

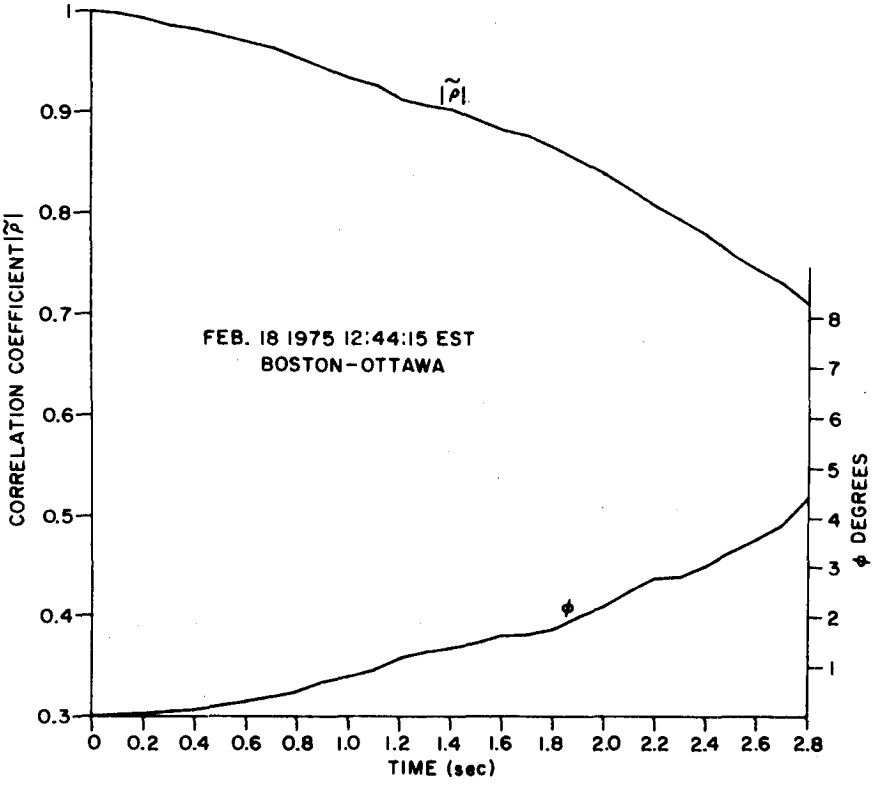

Figure 18. Plot of the Magnitude and Phase of the Complex Correlation Coefficient against Time from Data Obtained over the Boston-Ottawa Link on 18 February 1975, 12:44:15 EST.

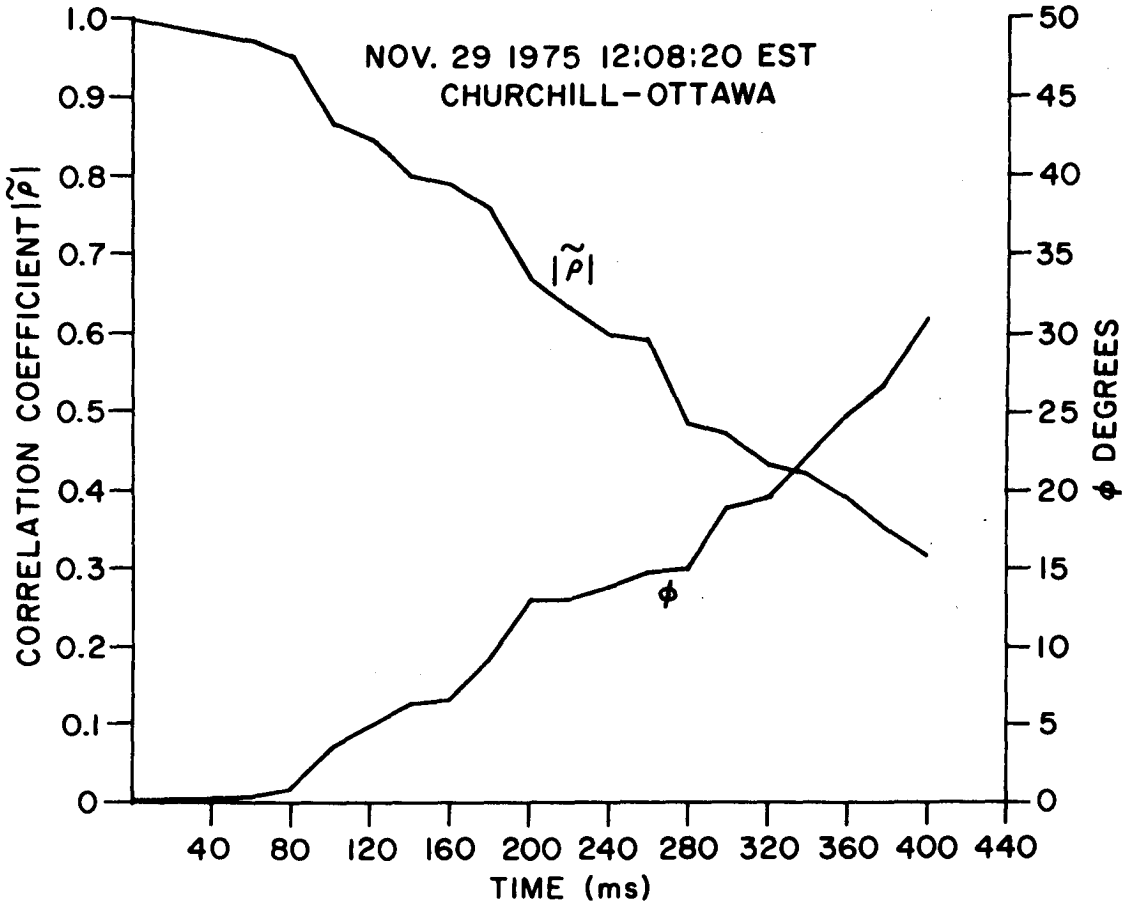

Figure 19. Plot of the Magnitude and Phase of the Complex Correlation Coefficient against Time from Data Obtained over the Churchill-Ottawa Link on November 29, 1975 12:08:20 EST.

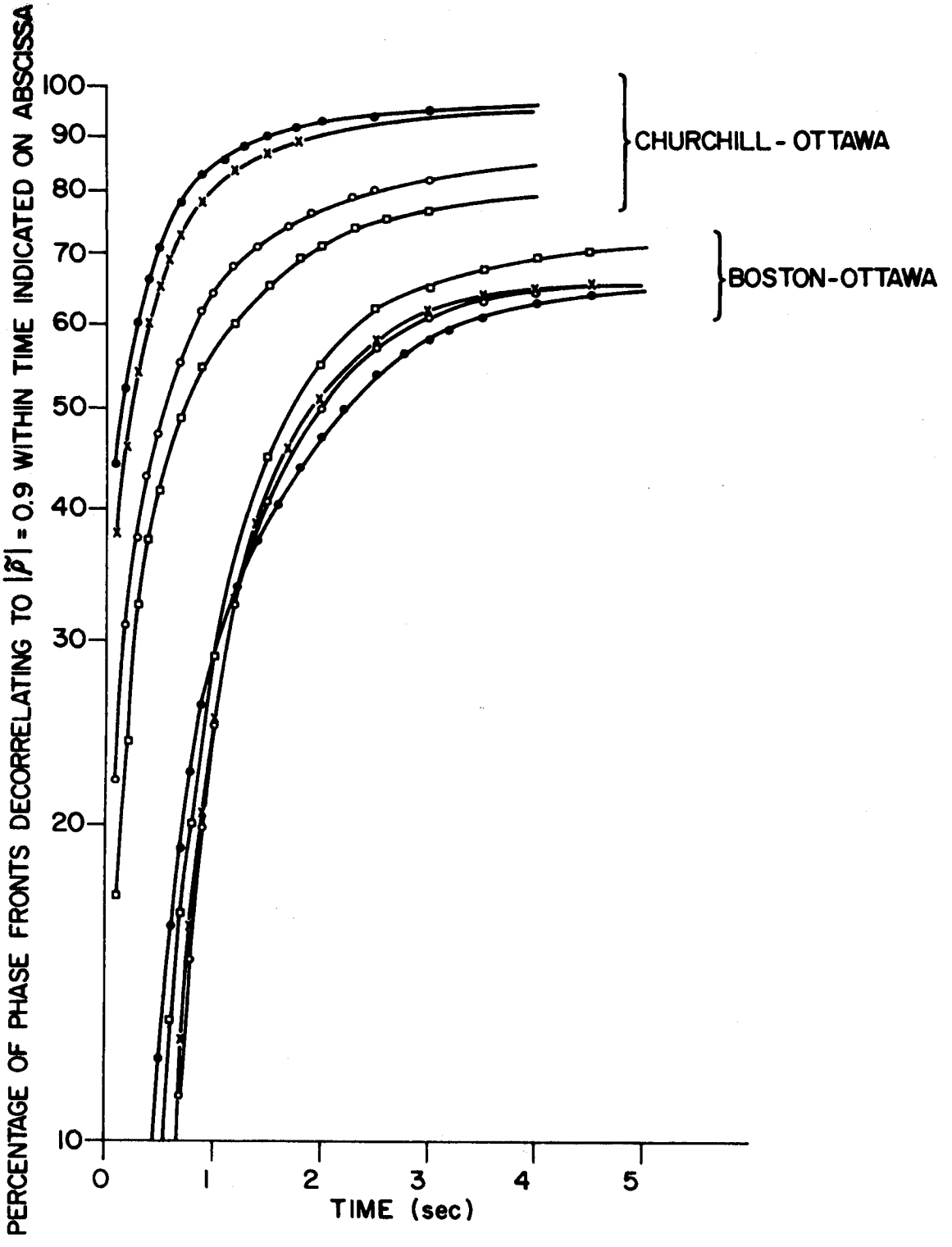

Figure 20. Cumulative probability distribution for time to decorrelate to $|\tilde{\rho}| = 0.9$. The four lines shown for each path are the results for each of four different days.

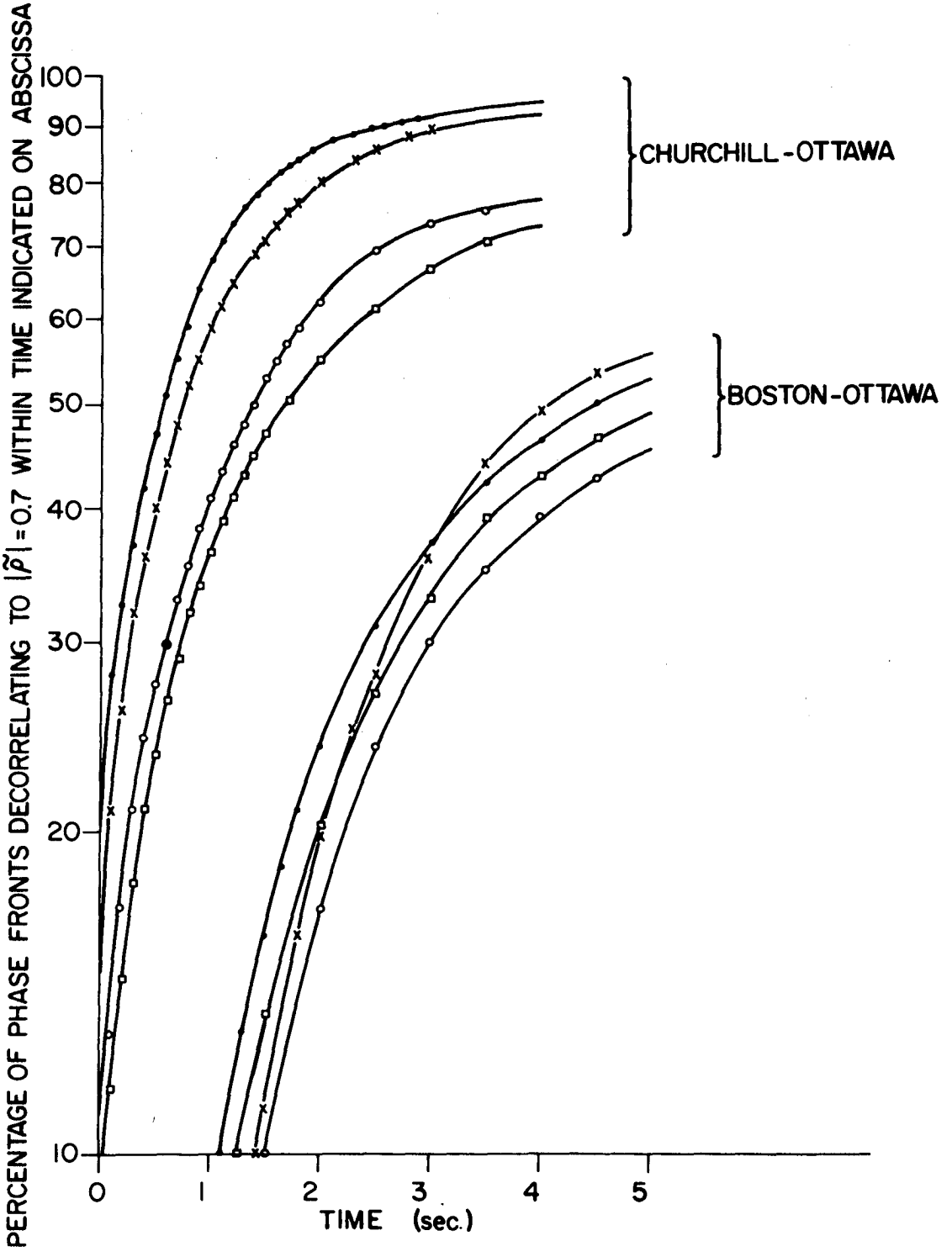

Figure 21. Cumulative probability distribution for time to decorrelate to $|\tilde{\rho}| = 0.7$. The four lines shown for each path are the results for each of four different days.

7. SUMMARY AND CONCLUSIONS

In general, there are three factors which cause changes in the detailed shape of wave-interference patterns of ionospherically-propagated radio waves. These three factors, namely, amplitude-change, phase-path change (Doppler shift), and angle-change, cause time variations in the instantaneous wavefronts, in turn reducing the ability of a direction-finder to determine the bearing of a source of transmission.

In the work reported here, it has been found that phase fronts on a short one-hop, mid-latitude path decorrelate with a characteristic time in the range 2-5 seconds, while, for a 1950 km sub-auroral path, decorrelation takes place in about one-fifth of the time.

8. ACKNOWLEDGEMENTS

Useful discussion with Dr. R.V. Webber and Dr. D.W. Rice is acknowledged. This work was sponsored by the Department of National Defence, under Research and Development Branch Project 3633G.

9. REFERENCES

1. Hayden, Edgar, C., *Propagation Studies Using Direction-Finding Techniques*. Journal of Research of the National Bureau of Standards, D. Radio Propagation, Vol. 65D, No. 3, May-June 1961, p. 197.

2. Rice, D.W., *Phase Characteristics of Ionospherically-Propagated Radio Waves*. Nature, Physical Science, Vol. 244, No. 136, pp. 86-88, 6 August 1973.

3. Rice, D.W. and E.L. Winacott, *A Sampling Array for H.F. Direction-Finding Research*, CRC Report No. 1310, October 1977.

4. *Reference Data for Radio Engineers*. Fifth Edition, Howard W. Sams and Co., New York, 1974, pp. 44-7.

APPENDIX I

General Solution for the Interference Pattern

Let there be two signals with wave vectors $\bar{k}_1$ and $\bar{k}_2$ (see Figure (I-1)) such that

$$|\bar{k}_1| = |\bar{k}_2| = k = \frac{2\pi}{\lambda} \tag{I-1}$$

then

$$S_1(x,y=0,t) = e^{j(k\ x\ \cos\psi_1 - \omega_1 t)} \tag{I-2}$$

and

$$S_2(x,y=0,t) = r\ e^{j(k\ x\ \cos\psi_2 - \omega_2 t)} \tag{I-3}$$

where $r < 1$. Thus, the sum of the two waves at a point on the x-axis is

$$S(x,t) = e^{j(k\ x\ \cos\psi_1 - \omega_1 t)} + r\ e^{j(k\ x\ \cos\psi_2 - \omega_2 t)} \tag{I-4}$$

where ω_1 and ω_2 are the carrier radian-frequencies of the two waves, assumed to be different, in general, because of the relative Doppler shifts.

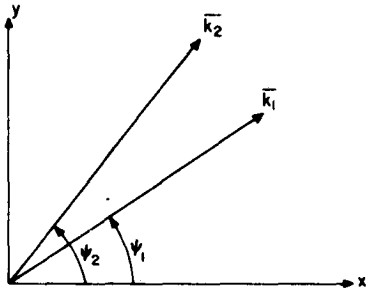

Figure I-1. Definition of Wave-Normal Directions with Respect to a Linear-Array along the X-Axis.

Let

$$\omega_1 = \omega_o \ , \ \omega_2 = \omega_o + \omega_d \tag{I-5}$$

where ω_d is the Doppler-shift radian frequency; then eqn. (I-4) may be written

$$S(x,t) = e^{-j\omega_o t}\left\{ e^{jkx \cos \psi_1} + r\, e^{j(kx \cos \psi_2 - \omega_d t)} \right\} \tag{I-6}$$

Let $S(x,t)$ be written in polar form

$$S(x,t) = a(x,t)\, e^{-j\omega_o t}\, e^{j\phi(x,t)} \tag{I-7}$$

Here we are interested in $\phi(x,t)$ only, since the amplitude information is discarded, and the carrier phase is of no consequence. Thus, $\phi(x,t)$ is given by

$$\tan \phi = \frac{r \sin (kx \cos \psi_2 - \omega_d t) + \sin (kx \cos \psi_1)}{r \cos (kx \cos \psi_2 - \omega_d t) + \cos (kx \cos \psi_1)} \tag{I-8}$$

Now, we have the following trignometric identities (see reference 4).

$$\left.\begin{aligned} \sin A + r \sin B &= \rho \sin C \\ \text{where} \qquad \rho^2 &= 1 + r^2 + 2r \cos (B - A) \\ \text{and} \qquad \tan(C-A) &= \frac{r \sin (B - A)}{1 + r \cos (B - A)} \end{aligned}\right\} \tag{I-9}$$

From these, it may also be shown that

$$\cos A + r \cos B = \rho \cos C \tag{I-10}$$

Hence, eqn. (I-8) has the alternate form

$$\tan(\phi - kx\cos\psi_1) = \frac{r\sin(kx[\cos\psi_2-\cos\psi_1] - \omega_d t)}{1 + r\cos(kx[\cos\psi_2-\cos\psi_1] - \omega_d t)} \qquad \text{(I-11)}$$

Note that $(\phi - kx\cos\psi_1)$ is the phase deviation of the phase ϕ from the linear phase variation $kx\cos\psi_1$ due to the stronger wave.

Determination of the Maximum Phase Deviation

From eqn. (I-11), let

$$\beta = \phi - kx\cos\psi_1,\ k'x = kx[\cos\psi_2-\cos\psi_1], \qquad \text{(I-12)}$$

and let $\omega_d t$ be zero for all t, then eqn. (I-11) may be written

$$\tan\beta = \frac{r\sin(k'x)}{1 + r\cos(k'x)} \qquad \text{(I-13)}$$

differentiate eqn. (I-13) w.r.t. k'x

$$\frac{d\beta}{d(k'x)} = \frac{r^2 + r\cos(k'x)}{\sec^2\beta\,(1 + r\cos(k'x))^2} \qquad \text{(I-14)}$$

For β to be a maximum value, $d\beta/d(k'x) = 0$, therefore

$$\cos(k'x) = -r \qquad \text{(I-15)}$$

Replacing cos(k'x) by -r in eqn. (I-13) results in

$$\tan\beta_{max} = \frac{r\sin(k'x)}{1 - r^2} \qquad \text{(I-16)}$$

Since $\sin(k'x) = [1 - \cos^2(k'x)]^{\frac{1}{2}}$, then

$$\tan\beta_{max} = \frac{r}{(1 - r^2)^{\frac{1}{2}}} \qquad \text{(I-17)}$$

and therefore

$$\sin \beta_{max} = r \tag{I-18}$$

Referring now to the diagram in Figure 2, if β_{max} is a solution, so is $-\beta_{max}$. Hence, in general

$$\beta_{max} = \pm \sin^{-1}(r) \tag{I-19}$$

A P P E N D I X II

Complex Correlation Coefficient for the Special Case of Equal Mode Amplitudes

From eqn. (I-11) in Appendix I, the general expression for phase deviation is

$$\tan \beta = \frac{r \sin(k'x - \omega_d t)}{1 + r\cos(k'x - \omega_d t)} \tag{II-1}$$

where

$$\beta = \phi - kx \cos\psi_1 \tag{II-2}$$

and

$$k' = k(\cos\psi_2 - \cos\psi_1) \tag{II-3}$$

In the limiting case of equal signal amplitudes, r=1, and eqn. (II-1), by a simple trigonometric identity, becomes

$$\beta = \frac{1}{2}(k'x - \omega_d t) \tag{II-4}$$

Figure II-1 shows the phase $\beta(x,t)$ at two different instants in time, t_1 and t_2. Note that the angle β is limited to the range $-\pi/2 \leq \beta \leq \pi/2$.

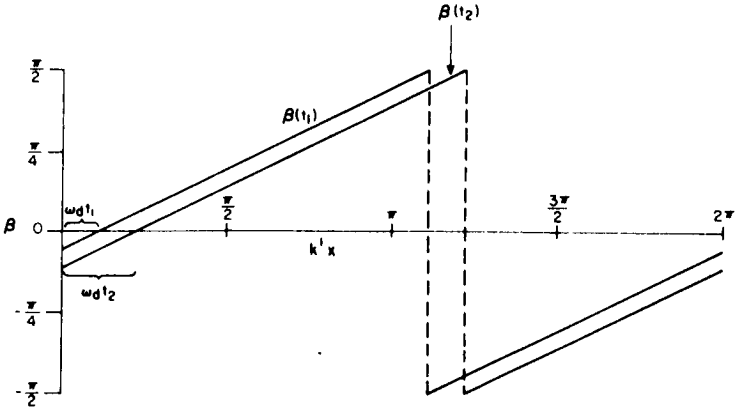

Figure II-1. Phase Deviation $\beta(x,t)$, at Two Particular Times t_1 and t_2, as a Function of the Normalized Spatial Variable k'x.

Representing the phases $\beta(x,t_1)$ and $\beta(x,t_2)$ in complex exponential form, the complex correlation coefficient $\tilde{\rho}$ is given by

$$\tilde{\rho}(t_1,t_2) = \frac{1}{L}\int_o^L e^{-j\beta(x,t_1)}\, e^{j\beta(x,t_2)}\, dx \qquad \text{(II-5)}$$

where L is taken as the length of one period in the interference pattern.

Changing the variable of integration to $\delta = k'x$,

$$\tilde{\rho}(t_1,t_2) = \frac{1}{2\pi}\int_o^{2\pi} e^{-j\frac{1}{2}(\delta-\omega_d t_1)}\, e^{j\frac{1}{2}(\delta-\omega_d t_2)}\, d\delta \qquad \text{(II-6)}$$

However, care must be exercised in evaluating the above integral, because of the restriction of the arguments of the complex exponentials to the range $(-\pi/2, \pi/2)$. From Figure II-1, it can be seen that eqn. (II-6) becomes

$$\tilde{\rho}(t_2-t_1) = \frac{1}{2\pi}\left\{\int_o^{\pi+\omega_d t_1} e^{-j\frac{1}{2}(\omega_d t_2-\omega_d t_1)}\, d\delta + \int_{\pi+\omega_d t_1}^{\pi+\omega_d t_2} e^{j\left[\pi-\frac{1}{2}(\omega_d t_2-\omega_d t_1)\right]}\right.$$

$$\left. + \int_{\pi+\omega_d t_2}^{2\pi} e^{-j\frac{1}{2}(\omega_d t_2-\omega_d t_1)}\, d\delta\right\} \qquad \text{(II-7)}$$

which results in

$$\tilde{\rho}(\tau) = 1 - \left[\frac{\omega_d\tau}{2}\right] e^{-j\frac{\omega_d\tau}{2}} \qquad 0 \le \tau \le \frac{2\pi}{\omega d} \qquad \text{(II-8)}$$

where (t_2-t_1) has been replaced by τ, which is the time interval between the two sets of complex phases. Finally, it is easily seen that $\tilde{\rho}(\tau)$ repeats beyond the range $(0, 2\pi/\omega_d)$.